Comparative studies of the structure, morphology and electrical conductivity of polyaniline weakly doped with chlorocarboxylic acids

2007 J. Phys.: Condens. Matter 19 326203

(http://iopscience.iop.org/0953-8984/19/32/326203)

IOP PUBLISHING JOURNAL OF PHYSICS: CONDENSED MATTER

J. Phys.: Condens. Matter **19** (2007) 326203 (13pp) doi:10.1088/0953-8984/19/32/326203

Comparative studies of the structure, morphology and electrical conductivity of polyaniline weakly doped with chlorocarboxylic acids

Fethi Gmati[1], **Arbi Fattoum**[1], **Nadra Bohli**[1], **Wadia Dhaoui**[2] **and Abdellatif Belhadj Mohamed**[1]

[1] Centre of Research and Technology of Energy, Laboratory of Photovoltaics and Semiconductors, Technopole of Borj Cedria, Hammam Lif 2050, Tunisia
[2] Research Unit of Physical Chemistry of Solid Materials, Faculty of Sciences, University of Tunis, Elmanar II 2092, Tunisia

Received 24 April 2007, in final form 11 June 2007
Published 13 July 2007
Online at stacks.iop.org/JPhysCM/19/326203

Abstract

We report the results of studies on two series of polyaniline (PANI), doped with dichloroacetic (DCA) and trichloroacetic (TCA) acids, respectively, at various doping rates and obtained by the *in situ* polymerization method. Samples were characterized by x-ray diffraction, scanning electron microscopy and conductivity measurements. The direct current (dc) and alternating current (ac) electrical conductivities of PANI salts have been investigated in the temperature range 100–310 K and frequency range 7–10^6 Hz. The results of this study indicate better chain ordering and higher conductivity for PANI doped with TCA. The dc conductivity of all samples is suitably fitted to Mott's three-dimensional variable-range hopping (VRH) model. Different Mott parameters such as characteristic temperature T_0, density of states at the Fermi level ($N(E_F)$), average hopping energy (W) and the average hopping distance (R) have been evaluated. The dependence of such values on the dopant acid used is discussed. At high frequencies, the ac conductivity follows the power law $\sigma_{ac}(\omega, T) = A(T)\omega^{s(T,\omega)}$, which is characteristic for charge transport in disordered materials by hopping or tunnelling processes. The observed increase in the frequency exponent s with temperature suggests that the small-polaron tunnelling model best describes the dominant ac conduction mechanism. A direct correlation between conductivity, structure and morphology was obtained in our systems.

1. Introduction

In the last decades, π-conjugated polymers have become a subject of experimental and theoretical intensified studies, because of the possibilities of their potential applications in

various domains. Amongst them, polyaniline (PANI) deserves much attention because of its good environmental stability, relatively high conductivity, and the possibility to be doped by a simple acid /base reaction using a protonic acid as the dopant.

The conductivity is largely affected by the nature of the doping acid and the doping rate [1–3]. Previously, various acids [3–18] have been used to protonate PANI, to enhance its conductivity, understand the effect of the dopant in the charge transport mechanisms, and correlate the structure and the properties.

By the doping process, polarons and bipolarons are generated [19], and they contribute to the conduction by phonon-assisted hopping or by tunnelling between electronic localized states randomly distributed. The variable-range hopping (VRH) conduction mechanism was originally proposed by Mott for amorphous semiconductors [20], assuming a phonon-assisted hopping process. However, this model is reported by previous studies to explain the charge transport in conducting polymers and their composites at low temperature [5, 6, 8, 11, 13, 17, 21–23]. The bulk conductivity of conducting polymers depends upon several factors, such as the structure, the number and the nature of charge carriers, and their transport along and between the polymer chains and across the morphological barriers [15, 24]. The ac conductivity measurements are used to give rich additional information about the conduction mechanism in conducting polymers that dc conductivity measurements alone do not provide [24–26]. Several theoretical models [20, 27, 28] have been proposed to explain the ac conduction mechanism in amorphous semiconductors [27–30], chalcogenide glasses [31], conducting polymers and their composites [24–26, 32].

The present work is a contribution to the previous studies concerning the electrical behaviour and structure of conducting polymers. The aim is to study and to compare the influence of the dopant acid on the structure, the morphology and the electrical conductivity of PANI weakly doped at various doping rates with dichloroacetic (DCA) and trichloroacetic (TCA) acids under the same synthesis conditions.

2. Experimental techniques

2.1. Sample preparation

Polyaniline (PANI) doped with dichloroacetic Cl_2CH–COOH (DCA) or trichloroacetic Cl_3C–COOH (TCA) acids (PANI-DCA and PANI-TCA) at different doping rates were synthesized by chemical oxidative polymerization of 0.2 M aniline (p.a. (pure aniline), Merck) in 0–2 M aqueous solutions of dichloroacetic or trichloroacetic acids with ammonium peroxydisulfate $(NH_4)_2S_2O_8$ (APS) (0.25 M) as the oxidant, in the temperature range 0–5 °C. A reactive mixture was made under constant stirring for 24 h. The precipitated PANI salt was separated by filtration, rinsed with a corresponding solution of acid and dried at ambient temperature in vacuum. A detailed synthesis process of PANI-DCA and PANI-TCA has been published by Dhaoui *et al* [18]. Samples will be denoted as S_1, S_2, S_3 for PANI doped with TCA at the doping rates 4.1%, 6.1%, 13.5% and S_4, S_5, S_6 for PANI doped with DCA at the doping rates 6.1%, 8.2%, 13.3%.

2.2. Characterization techniques

X-ray diffraction (XRD) measurements were carried out by using a PANalytical/X'Pert Pro MPD x-ray diffractometer using Cu Kα radiation ($\lambda = 1.5418$ Å) in the 2θ range 0°–40° on powdered samples. The scanning electron microscopy (SEM) micrographs were obtained from a Philips XL 30 scanning electron microscope operating at 20 kV. Conductivity measurements

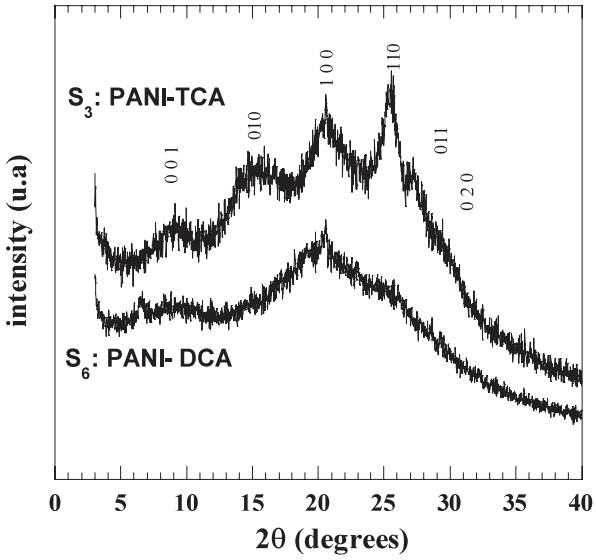

Figure 1. The x-ray diffraction patterns for S_3: PANI-TCA (13.5%), and S_6: PANI-DCA (13.3%).

were recorded on pressed pellets of a uniform thickness $t = 1.5$ mm and diameter $d = 13$ mm in the temperature range 100–310 K and frequency range 7–10^6 Hz. The dc conductivity measurements were performed using an Agilent multimeter 34401A, by measuring the bulk resistance R of the sample, and employing the formula $\sigma_{dc} = \frac{1}{R}\frac{t}{S}$, where t and S are the thickness and the surface area. The ac conductivity is deduced from the measurement of the impedance $Z(\omega) = Z'(\omega) + iZ''(\omega)$, using an HP4192 A LF impedance analyser. The system is described by an equivalent RC parallel circuit [33]. The relative complex permittivity of the material is defined by $\varepsilon_r^*(\omega) = \varepsilon_r'(\omega) - i\varepsilon_r''(\omega)$, where $\varepsilon_r''(\omega)$ describes the global loss factor in the material and is given by $\varepsilon_r''(\omega) = \frac{1}{C_0\omega}\frac{Z'}{Z'^2+Z''^2}$, where $C_0 = \frac{\varepsilon_0 S}{t}$ is the capacity with a free space between the electrodes, ε_0 is the permittivity of a vacuum, and $\omega = 2\pi F$ is the angular frequency of the applied electric field. The ac conductivity $\sigma(\omega)$ has been calculated from the global loss factor according to the following relation:

$$\sigma^*(\omega) = j\omega\varepsilon_o\varepsilon_r^*(\omega) = j\omega\varepsilon_o(\varepsilon_r'(\omega) - j\varepsilon_r''(\omega)) = \omega\varepsilon_o\varepsilon_r''(\omega) + j\omega\varepsilon_o\varepsilon_r'(\omega).$$

3. Results and discussion

The x-ray diffraction (XRD) patterns of S_3 (PANI-TCA 13.5%) and S_6 (PANI-DCA 13.3%) are presented in figure 1. Diffraction peaks that are relatively sharp and strong at $2\theta = \sim 4.7°, 9.2°$, 14.7°, 20.4°, 25.5° and 29.2° are visible in the PANI-TCA pattern. These peaks are compatible with the pseudo-orthorhombic lattice symmetry [18, 34]. The relevant crystal planes are indicated inset. In contrast, PANI-DCA shows an appreciable loss in crystallinity which results in the disappearance or broadening of the diffraction peaks at $2\theta = \sim 14.7°$, 20.4°, 25.5° and 29.2°, implying a decrease in coherence length of the polymer chain. These results reveal that the crystallinity of the doped polymer depends on the nature of the dopant counter-ion which can undergo secondary interaction inducing a higher degree of chain ordering [18, 34].

The effect of the dopant is also visible on the polymer morphology. In fact, SEM micrographs revealed a granular structure for PANI-TCA (figure 2(a)) in contrast to the sponge-like structure derived from aggregation of small granules for PANI-DCA (figure 2(b)).

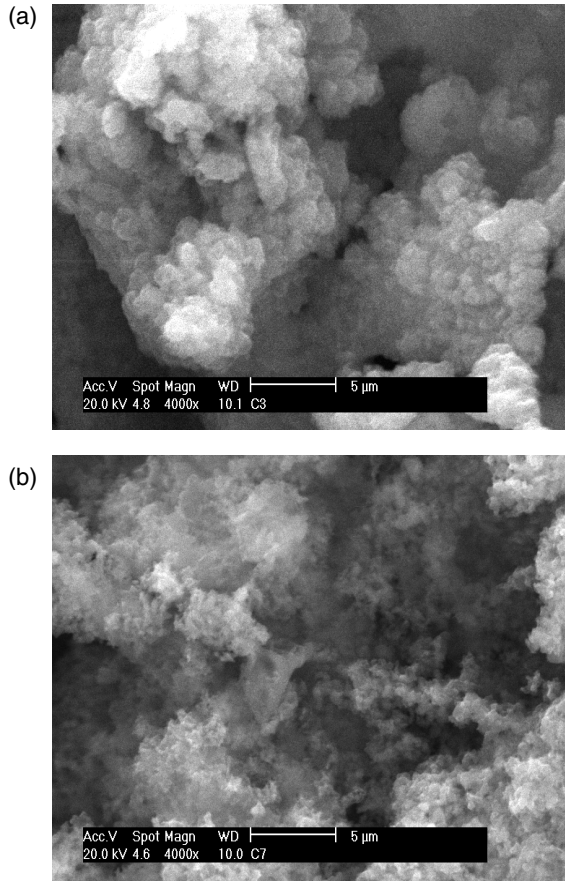

Figure 2. Scanning electron micrographs for PANI-TCA (a) and PANI-DCA (b) at magnification 4000×.

The variation of the dc conductivity, σ_{dc}, with temperature is represented for PANI-TCA in figure 3(a) and for PANI-DCA in figure 3(b). The observed increase in σ_{dc} with temperature indicates semiconductor behaviour [6–13] for both PANI-TCA and PANI-DCA salts. In addition, the dc conductivity of both series increases on increasing the doping rate; this may be due to the increase in the number of polarons formed during the doping process [1, 12], which causes an increase in conductivity not only by increasing the carrier concentration but also by increasing the mobility which renders the interchain charge transport more efficient [11]. For the same doping rate (S_2 compared with S_4 and S_3 compared with S_6) PANI-TCA remains more conductive than PANI-DCA.

We have fitted the conductivity data of PANI salt samples by using several conduction models [9]. The best fits were obtained with the 3D VRH conduction model. In this model, when the interaction between charge carriers is neglected, the dc conductivity is expressed as follows [20]:

$$\sigma_{dc} = B(T_0/T)^{1/2} \exp[-(T_0/T)^{1/4}] \tag{1}$$

where B is a constant depending on the distribution of localized states around the Fermi level and is given by [20]

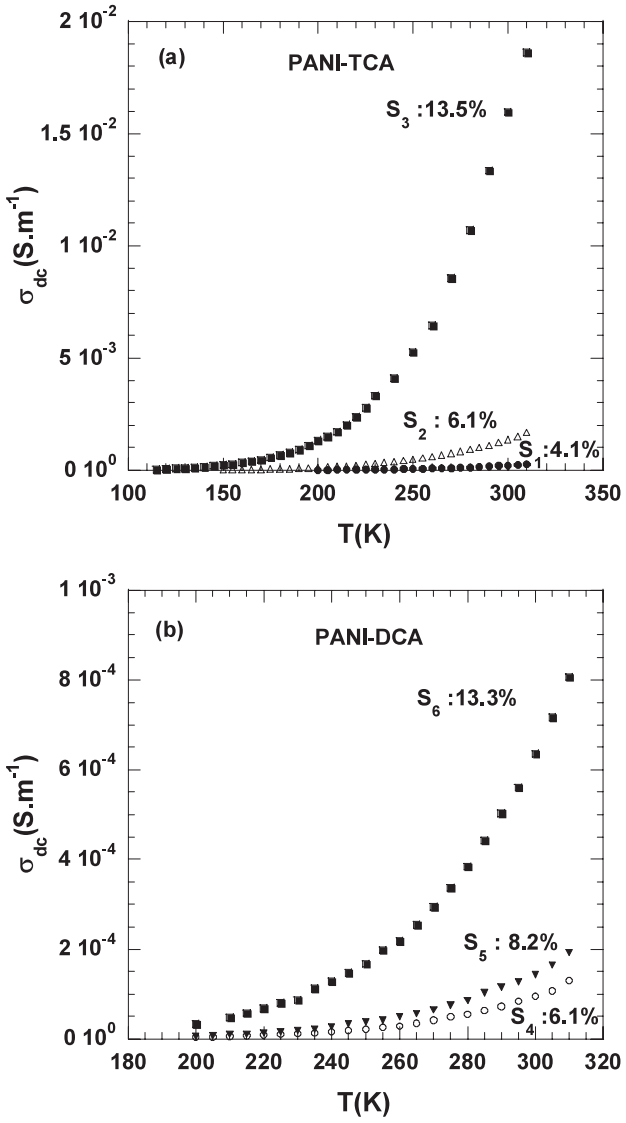

Figure 3. Variation of dc conductivity (σ_{dc}) versus temperature for PANI-TCA salts S_1, S_2 and S_3 (a) and PANI-DCA salts S_4, S_5 and S_6 (b).

$$B = N(E_F)e^2\nu_{ph}\frac{9}{64\alpha^2} \tag{2}$$

where $N(E_F)$ is the density of states at the Fermi level, ν_{ph} is the phonon frequency ($\approx 10^{13}$ Hz), e is the electronic charge and $1/\alpha$ is the decay length of the localized wavefunction.

T_0 is the characteristic Mott temperature; it corresponds to the hopping barrier for charge carriers (also known as the pseudo-activation energy) and measures the degree of disorder present in the system, and it is given by [20]

$$T_0 \cong 18.11\frac{\alpha^3}{N(E_F)k_B}. \tag{3}$$

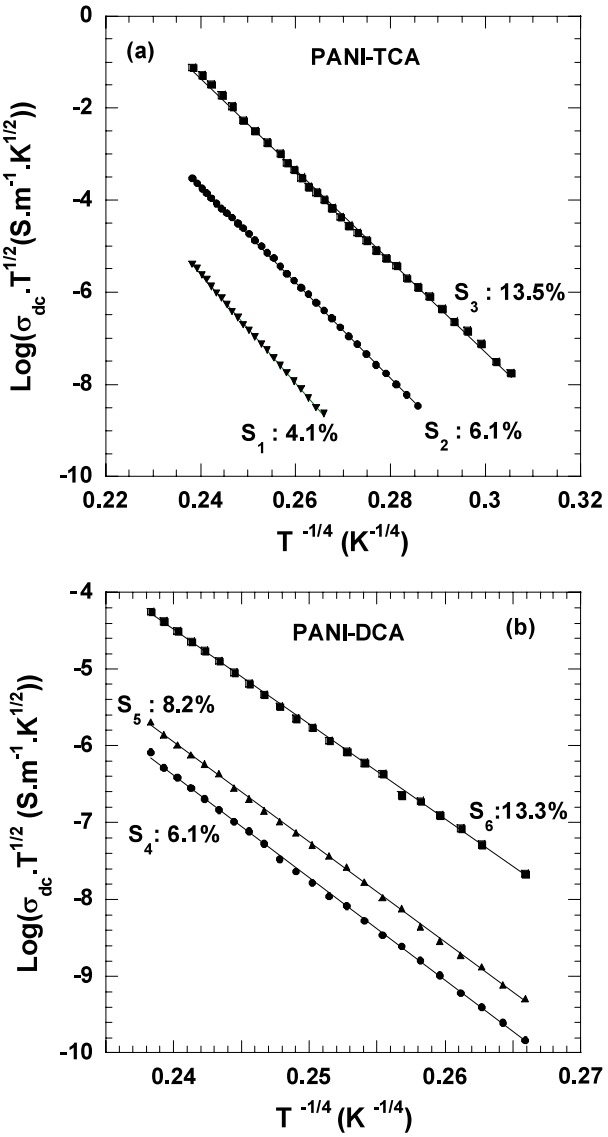

Figure 4. Variation of dc conductivity ($\log(\sigma_{dc}T^{1/2})$) versus temperature ($T^{-1/4}$) for S_1, S_2 and S_3 (a) and for S_4, S_5 and S_6 (b) (the solid lines are data fitted to the 3D VRH model).

The average hopping distance and the average hopping energy are given respectively by [20]

$$R = \left[\frac{9}{8\alpha\pi N(E_F)k_BT}\right]^{1/4} \tag{4}$$

and

$$W = \frac{3}{4\pi N(E_F)R^3}. \tag{5}$$

In figures 4(a) and (b) we have plotted $\log(\sigma_{dc}T^{1/2})$ versus $T^{-1/4}$ for both series of salts (PANI-TCA and PANI-DCA respectively), and in figure 5 for the two samples S_2 and S_4 having

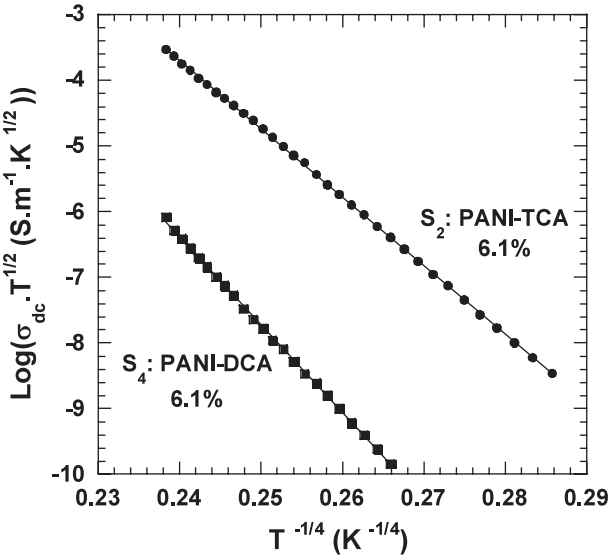

Figure 5. Variation of dc conductivity ($\log(\sigma_{dc}T^{1/2})$) versus temperature ($T^{-1/4}$) for S_2 and S_4 doped at the same rate 6.1% with TCA and DCA respectively (the solid lines are data fitted to the 3D VRH model).

Table 1. Mott parameters of polyaniline doped with TCA.

Sample	Doping rate (%)	σ_{dc} (S m^{-1}) 300 K	T_0 (K)	$N(E_F)$ (eV^{-1} cm^{-3})	R (300 K) (nm)	W (300 K) (meV)	R (200 K) (nm)	W (200 K) (meV)
S_1	4.1	2.1×10^{-4}	1.97×10^{8}	8×10^{17}	11.74	184	12.99	136
S_2	6.1	1.3×10^{-3}	1.18×10^{8}	13.37×10^{17}	10.32	162	11.43	120
S_3	13.5	1.6×10^{-2}	0.97×10^{8}	16.3×10^{17}	9.83	154	10.9	113

Table 2. Mott parameters of polyaniline doped with DCA.

Sample	Doping rate (%)	σ_{dc} (S m^{-1}) 300 K	T_0 (K)	$N(E_F)$ (eV^{-1} cm^{-3})	R (300 K) (nm)	W (300 K) (meV)	R (200 K) (nm)	W (200 K) (meV)
S_4	6.1	1×10^{-4}	3.19×10^{8}	4.94×10^{17}	13.25	207	14.66	154
S_5	8.2	1.4×10^{-4}	2.89×10^{8}	5.44×10^{17}	12.93	203	14.31	150
S_6	13.3	6.4×10^{-4}	2.33×10^{8}	6.77×10^{17}	12.24	192	13.55	142

the same doping rate (6.1%). The linear behaviour of the plots indicates that the 3D VRH mechanism dominates in the temperature range of study. The slopes of the straight lines give the value of T_0 for each sample (see tables 1 and 2). It is clear that T_0 decreases for each series when the doping rate is increased and takes lower values in the case of PANI-TCA when the same doping rate is considered (S_4 compared with S_2 and S_6 compared with S_3).

Various Mott parameters calculated from equations (1)–(3), assuming α^{-1} to be 1.1 nm [5], and evaluated at 300 K and 200 K, are listed respectively in tables 1 and 2. It is clear from tables 1 and 2 that the density of localized states $N(E_F)$ increases when the doping rate is increased; this may be attributed to the formation of new states responsible for charge

Table 3. Variation with temperature of Mott parameters for S_3.

T (K)	R (nm)	W (meV)	k_BT (meV)	$R\alpha$
300	9.83	154	25.9	8.9
200	10.9	113	17.3	9.9
120	12.4	78	10.4	11.2

transport [5, 11, 22]. On the other hand, the average hopping distance R, the average hopping energy W and the size of the hopping barrier T_0 decrease; this enhances hops between adjacent localized states and leads to an increase in conductivity.

The molecular size of the dopant can strongly affect the conformation of PANI chains and their coupling. In fact, the TCA^- counter-ion ($Cl_3C–COO^-$) is larger in size than DCA^- ($Cl_2CH–COO^-$); it can stop the twist and the cross-linking of PANI chains, keeping them in more expanded conformation [15, 18] which allows better chain ordering and then higher conductivity in PANI-TCA than in PANI-DCA. This result is in accordance with the literature indicating that the conductivity increases with increasing the volume of the dopant counter-ion [14, 18]. Similar behaviour has been observed in PANI doped with other acids [5, 13, 15] and in other doped conjugated polymers [21–23].

We give in table 3 the variations with temperature of the Mott parameters of sample S_3. It is evident from this table that $R\alpha > 1$ and $W > k_BT$, which agree with Mott's condition for variable range hopping. In fact, $R\alpha$, called the degree of localization, is found to be ≈9.9 for S_3 and ≈12.32 for S_6 at $T = 200$ K. This indicates that the charge carriers are highly localized in both salts, but more localized in PANI-DCA since $R\alpha$ is higher. This explains the poor conducting behaviour of the systems, especially for PANI-DCA. It is also visible from table 3 that when the temperature decreases, the average hopping energy W decreases and the average hopping distance R increases, which supports that when the phonon energy is insufficient (low temperature), carriers will tend to hop larger distances in order to locate in sites which are energetically closer than their nearest neighbours. Similar behaviour of $R\alpha$ is expected for all samples and over the whole temperature range of study.

The conductivity in alternative current is plotted in order to obtain additional information about charge transport in our samples. The $\log\sigma$ versus $\log\omega$ plots at different temperatures are given in figures 6(a) and (b) for S_3 and S_6 respectively. It can be seen that the conductivities of PANI-TCA and PANI-DCA are both frequency and temperature dependent. The curves exhibit two distinct regions: a low-frequency region and a high-frequency one. At low frequencies, a plateau is present; it characterizes the dc conductivity, i.e. at a given temperature the total $\sigma(\omega, T)$ maintains a constant value ($\sigma(\omega, T) = \sigma_{dc}(T)$) up to a critical angular frequency ω_c, at which it begins to increase monotonically. At high frequencies ($\omega > \omega_c$) the conductivity follows an apparent power law: $\sigma(\omega, T) \approx \sigma_{ac}(\omega, T) \approx A(T)\omega^{s(T,\omega)}$, where the factor A depends on temperature and the exponent s lies between 0 and 1. Similar behaviour has been observed in PANI doped with other dopants [5, 35], its derivatives [1], and other conducting polymers [19, 24, 25].

The total conductivity of PANI-TCA and PANI-DCA is suitably described by the Jonscher universal power law [36]:

$$\sigma(\omega, T) = \sigma_{dc}(T) + A(T)\omega^{s(T,\omega)}. \tag{6}$$

The angular frequency exponent s follows the relation [20]

$$s = \frac{\mathrm{dLn}\sigma_{ac}(\omega)}{\mathrm{dLn}\omega}, \tag{7}$$

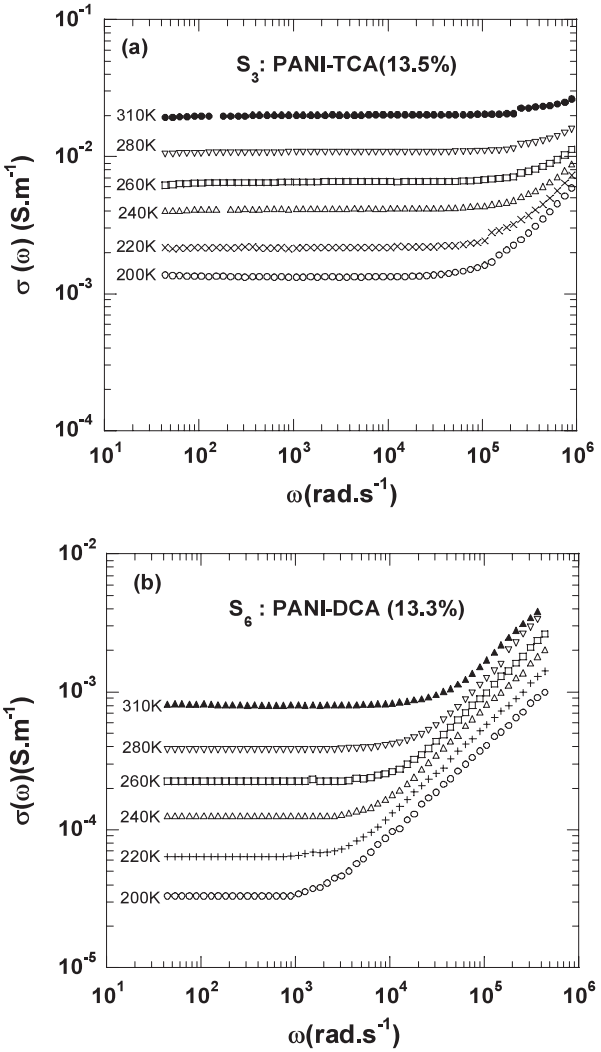

Figure 6. Angular frequency dependence of the conductivity ($\log \sigma$ versus $\log \omega$) for S_3 (a) and for S_6 (b) at various temperatures indicated inset.

Table 4. Variation of the exponent s with doping rate for PANI-TCA and PANI-DCA at 250 K.

	Sample	Doping rate (%)	Exponent s
PANI-TCA	S_2	6.1	0.85
	S_3	13.5	0.73
PANI-DCA	S_5	8.2	0.55
	S_6	13.3	0.38

and it is obtained from the slope of the solid line in the plot of $\log \sigma_{ac}$ versus $\log \omega$ (figures 7(a) and (b)). At a given temperature and a fixed angular frequency range, the exponent s of both PANI-TCA and PANI-DCA decreases when the doping rate is increased (table 4). This result is in good agreement with that obtained by Singh and Chandra for PANI-HCI [5].

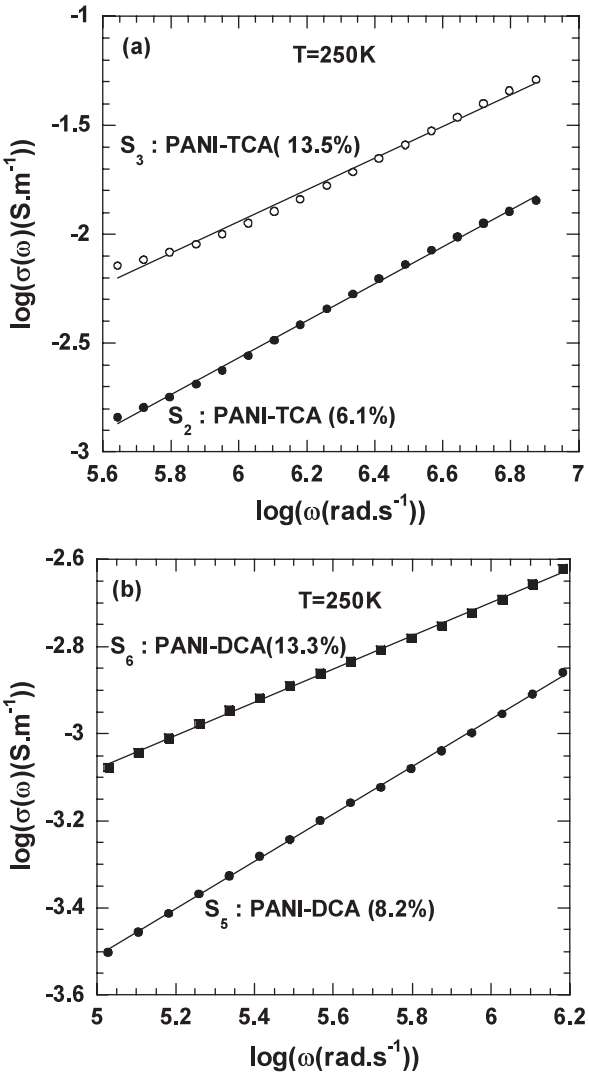

Figure 7. Angular frequency dependence ($\log\sigma$ versus $\log\omega$) at $T = 250$ K in the frequency range dominated by the power law $\sigma_{ac}(\omega) = A\omega^s$, for S_5, S_6 (a) and for S_2, S_3 (b).

The charge transport process in disordered solids in the presence of alternating field can be described by different models such as correlated barrier hopping (CBH) [27], electron tunnelling (quantum mechanical tunnelling (QMT)) [20], small polaron tunnelling, large polaron tunnelling [27] and random free-energy barrier (symmetric hopping model) [28].

In aiming to determine the compatible mechanism of charge transport in our samples, we have plotted the temperature dependence of s for sample S_2 (figure 8). It is clear that s increases with temperature. This behaviour is reproducible in all samples. In the QMT model, the exponent s remains almost equal to 0.8 or increases slightly with increasing temperature [20]; it may not be applicable for explaining the obtained results of the present study. In the CBH model, the exponent s decreases with increasing temperature; consequently, this model is also not applicable for explaining our results. The increase of s with temperature implies that the

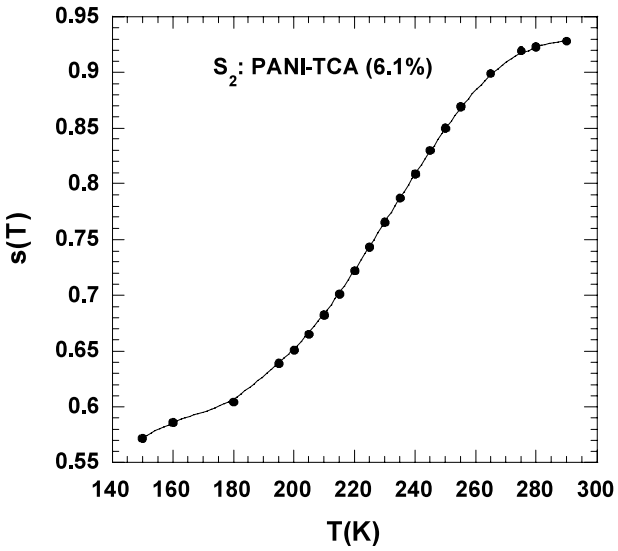

Figure 8. Temperature dependence of the exponent s for S_2.

small-polaron tunnelling model may be a possible theory to explain the conduction mechanism in our PANI-TCA and PANI-DCA.

The ac conductivity in the small-polaron tunnelling model is given by [27]

$$\sigma_{ac}(\omega) = \frac{\pi^4}{12}\frac{e^2 k_B T[N(E_F)]^2}{2\alpha}\omega R_\omega^4 \tag{8}$$

where R_ω is the tunnel distance at the angular frequency ω and is given by [27]

$$R_\omega = -\frac{1}{2\alpha}\left[\mathrm{Ln}(\omega\tau_{0p}) + \frac{W_H}{k_B T}\right]. \tag{9}$$

The frequency exponent s in this model is given by [27]

$$s = 1 + \frac{4}{\mathrm{Ln}(\omega\tau_{0p}) + W_H/k_B T} \tag{10}$$

where τ_{0p} is the time relaxation of the polaron (of the order of 10^{-13} s) [27] and W_H is the activation energy involved in the electron transfer process between a pair of states $W_H \approx W_p/2$ [20, 27], where W_p is the energy decrease associated with the lattice deformation at an occupied site (the polaron energy). W_H is evaluated from equation (10); for S_2, $W_H = 0.087$ eV.

The temperature and frequency dependence of R_ω for S_2 is shown in figure 9. It is seen that R_ω increases with temperature but becomes shorter when the frequency increases; this explains why at higher frequency the conductivity increases. When an alternative voltage is applied to a material, the charge carrier scans a distance that scales with the period of the electrical field. At low frequency, within one period, the electrical field forces the charge carrier to drift over a large distance; for example, at the frequency $F = 10$ Hz ($\omega = 62.8$ rad s^{-1}), the tunnelling distance R_ω for the sample S_2 at $T = 200$ K calculated from equation (9) is 11.43 nm, which is close to the average hopping distance R deduced from dc measurements (table 1). In contrast, in the high-frequency range, the mean displacement of the charge carrier is reduced; for example, at $F = 1.7 \times 10^5$ Hz ($\omega = 1.68 \times 10^6$ rad s^{-1}), the tunnel distance R_ω is 6.1 nm for S_2 at $T = 200$ K) (table 5), i.e. the charge carrier is only able to hop over a smaller distance compared to that at low frequency. This behaviour of R_ω is obtained for all our samples and

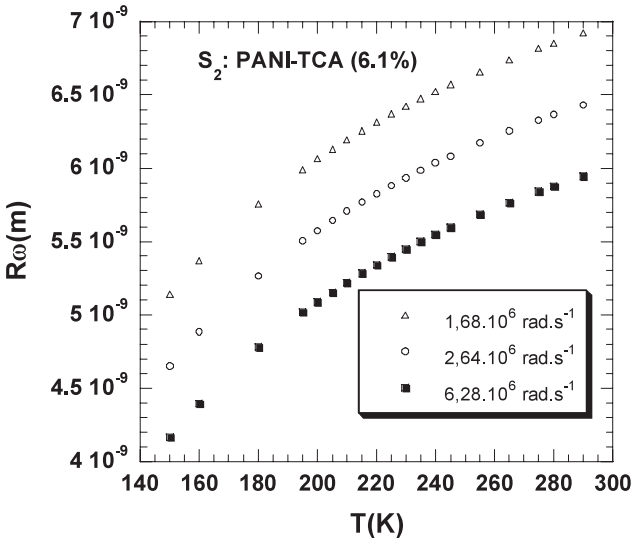

Figure 9. The temperature dependence of the tunnelling distance R_ω for S_2 at three representative frequencies in the region dominated by the power law ($\sigma_{ac}(\omega) = A\omega^s$).

Table 5. Frequency dependence of σ_{ac} and $N(E_F)$ measured at 200 K for S_2.

Angular frequency ω (rad s^{-1})	1.68×10^6	2.64×10^6	6.28×10^6
(R_ω) (m)	6.1×10^{-9}	5.6×10^{-9}	5.1×10^{-9}
σ_{ac} (S m^{-1})	6.25×10^{-3}	11.1×10^{-3}	20.2×10^{-3}
$N(E_F)$ (eV^{-1} cm^{-3})	5.91×10^{20}	5.97×10^{20}	6.24×10^{20}

may explain why the conductivity remains constant at low frequencies ($\sigma(\omega, T) = \sigma_{dc}(T)$) and increases at high frequencies.

The density of states $N(E_F)$ estimated from the ac data (table 5) are higher than values obtained from the dc data; these values ($N(E_F) \approx 10^{20}$ eV^{-1} cm^{-3}) are reasonable and in good agreement with the values obtained for conducting polyaniline [37, 38] and several disordered materials [20]. The observed increase in $N(E_F)$ when the frequency is increased is compatible with the observed increase in conductivity in the high-frequency range.

4. Conclusion

Polyaniline (PANI) doped with dichloroacetic (DCA) and trichloroacetic (TCA) acids was synthesized by the *in situ* polymerization method. Structural and morphological studies showed more crystalline PANI when doped with TCA, which is attributed to the favourable role of the TCA counter-ion in the better chain ordering. The conductivity increases by increasing the doping rate for both salts, and PANI-TCA is also found to be more conductive than PANI-DCA. The charge transport in direct current in both salts is well represented by the 3D Mott VRH model. The evaluated Mott parameters allowed us to attribute a higher influence of the dopant on the conductivity in the case of TCA.

The ac conductivity in the high-frequency range obeys the power law $\sigma_{ac}(\omega, T) = A(T)\omega^{s(T,\omega)}$, in which the angular frequency exponent s increases with temperature, suggesting that the small-polaron tunnelling model best describes the dominant ac conduction mechanism.

When the frequency is decreased, the evaluated tunnel distance increases and become close to the average hopping distance that is characteristic of dc conduction.

References

[1] Pinto N J, Sinha G P and Aliev F M 1998 *Synth. Met.* **94** 199–203
[2] Mac Diarmid A G 2002 *Synth. Met.* **125** 11–22
[3] Kahol P K, Ho J C, Chen Y Y, Wang C R, Neeleshawar S, Tsai C B and Wessling B 2005 *Synth. Met.* **151** 65–72
[4] Colak N and Sokmen B 2000 *Desig. Monom. Polym.* **2** 181–9
[5] Singh R, Arora V, Tandon R P and Chandra S 1998 *J. Mater. Sci.* **33** 2067–72
[6] Ghosh M, Meikap A K, Chattopadhyay S K and Chatterjee S 2001 *J. Phys. Chem. Solids* **62** 475–84
[7] Ghosh M, Barman A, Meikap A K, De S K and Chatterjee S 1999 *Phys. Lett.* A **260** 138–48
[8] Ghosh M, Barman A, De S K and Chatterjee S 1998 *Synth. Met.* **97** 23–9
[9] Mzenda V M, Goodman S A and Auret F D 2002 *Synth. Met.* **127** 285–9
[10] Rannou P, Wolter A, Travers J P, Gilles B and Djurado D 1998 *J. Chem. Phys.* **95** 1396–9
[11] Luthra V, Singh R, Gupta S K and Mansingh A 2003 *Curr. Appl. Phys.* **3** 219–22
[12] Blinova N V, Stejskal J, Trcova M and Prokes J 2006 *Polymer* **47** 42–8
[13] Wang J and Wan M X 1999 *Synth. Met.* **101** 846–7
[14] Mukh A K and Menon R 2002 *Pramana J. Phys.* **58** 238–9
[15] Long Y, Chen Z, Wang N, Zhang Z and Wan M 2003 *Physica* B **325** 208–13
[16] Long Y, Chen Z, Wang N, Li J and Wan M 2004 *Physica* B **344** 82–7
[17] Huang J and Wan M 1998 *Solid State Commun.* **108** 255–9
[18] Dhaoui W, Hbaieb S, Zarrouk H and Mohamed A B 2006 *Int. J. Polym. Anal. Charact.* **11** 239–52
[19] Capaccioli S, Lucchesi M, Rolla P A and Ruggeri G 1998 *J. Phys.: Condens. Matter* **10** 5595–617
[20] Mott N F and Davis E A 1979 *Electronic Processes in Non-Crystalline Materials* (Oxford: Clarendon) pp 157–60
[21] Singh R, Kaur A, Yadav K L and Bhattacharya D 2003 *Curr. Appl. Phys.* **3** 235–8
[22] Kaynak A 1998 *J. Chem.* **22** 81–5
[23] Maddison D S and Tansley T L 1992 *Appl. Phys.* **72** 4677–82
[24] Dutta P and De S K 2003 *Synth. Met.* **139** 201–6
[25] Suri K, Annapoorni S and Tandon R P 2003 *J. Non-Cryst. Solids* **332** 279–85
[26] De S, De A, Das A and De S K 2005 *Mater. Chem. Phys.* **91** 477–83
[27] Long A R 1982 *Adv. Phys.* **31** 553–637
[28] Dyre J C and Schroder T B 2000 *Rev. Mod. Phys.* **72** 873–873
[29] Long A R and Balkan N 1980 *J. Non-Cryst. Solids* **35-36** 415–20
[30] Okutan M, Basaran E, Bakan H I and Yakuphanoglu F 2005 *Physica* B **364** 300–5
[31] Elliott S R 1977 *Phil. Mag.* **36** 1291–304
[32] Gmati F, Fattoum A, Mohamed A B, Zangar H, Outzourit A and Achour M S 2006 *Phys. Chem. News* at press
[33] Soares B G, Leyva M E, Barra G M O and Khastgir D 2005 *Eur. Polym. J.* **42** 676–86
[34] Sai Ram M and Palaniappan S 2004 *J. Mater. Sci.* **39** 3069–77
[35] Dutta P, Biswas S and De S K 2001 *J. Phys.: Condens. Matter* **13** 9187–96
[36] Jonscher A K 1983 *Dielectric Relaxation in Solids* (London: Chelsea Dielectric press) chapter 3, p 89
[37] Alig I, Dudkin S M, Jenninger W and Marzantowicz M 2006 *Polymer* **47** 1722–31
[38] Nazeer K P, Thamilslvan M, Mangalaraj D, Narayandass Sa K and Yi J 2006 *J. Polym. Res.* **13** 17–23